Detonation Wave Diffraction in H_2-O_2-Ar Mixtures

S. Gallier[a], F. Le Palud[a,b], F. Pintgen[c], **R. Mével**[d], J.E. Shepherd[d]

[a]*SAFRAN-Herakles, Le Bouchet Research Center, 91710 Vert le Petit, France*

[b]*ISAE-SUPAERO, 10 avenue Édouard-Belin, 31055 Toulouse, France*

[c]*Cheniere Energy Inc., 700 Milam St, Houston, 77002 TX, USA*

[d]*California Institute of Technology, 1200 E California Blvd, Pasadena, 91125 CA, USA*

Corresponding Author

R. Mével

California Institute of Technology

1200 E. California Blvd. MC 105-50

Pasadena, CA 91125 USA

Tel.:+1 626 395 4755

Fax:+1 626 395 2900

E-mail: mevel@caltech.edu

Colloquium

Detonations, Explosions and Supersonic Combustion

Word count

Method: 1

Text = 3519 words

Equations = (2+4)*7.6*1 = 46 words

References = (45+2)*2.3*7.6 = 822 words

Figures = [(113+10)*2.2*1+33] + [(138+10)*2.2*1+32] + [(58.9+10)*2.2*2+34] + [(57.9+10)*2.2*1+25] + [(90.2+10)*2.2*1+41] + [(57.9+10)*2.2*1+21] = 1640 words

TOTAL length of paper: 6025 words

Abstract: 149 words

Color printing: we are not willing to pay charges for color printing

---

Abstract

In the present study, we have examined the diffraction of detonation in weakly unstable hydrogen-oxygen-argon mixtures. High accuracy and computational efficiency are obtained using a high-order WENO scheme together with adaptive mesh refinement, which enables handling realistic geometries with resolution at the micrometer level. Both detailed chemistry and spectroscopic models of laser induced fluorescence and chemiluminescence were included to enable a direct comparison with experimental data. Agreement was found between the experiments and the simulations in terms of detonation diffraction structure both for sub-critical and super-critical regimes. The predicted wall reflection distance is about 12-14 cell widths, in accordance with previous experimental studies. Computations show that the re-initiation distance is relatively constant, at about 12-15 cell widths, slightly above the experimental value of 11 cell widths. The predicted critical channel height is 10-11 cell widths, which differs from experiments in circular tubes but is consistent with rectangular channel results.

Keywords: Detonation diffraction, Adaptive mesh refinement, Planar laser-induced-fluorescence, Chemiluminescence, Hydrogen-oxygen mixtures

1. Introduction

As a detonation wave propagates from a confined channel to an unconfined space, it undergoes diffraction, which is characterized by a change of geometry from a quasi-planar wave to a cylindrical or spherical wave [1, 2, 3, 4]. Depending on the mixture composition, thermodynamic conditions, detonation velocity at the channel exit, the geometry of the area expansion and channel cross section, the detonation wave can be either extinguished (sub-critical regime) or re-initiated (super-critical regime) [2]. Detonation diffraction has been extensively studied both experimentally and through numerical simulations.

Since Zeldovich et al.'s pioneering work [5], numerous studies have been performed on detonation diffraction using a variety of experimental geometry and techniques, as summarized by Schultz [4] in 2000. Since then, a number of investigations have been performed, for example by Khasainov et al. [6], Meredith et al. [7], and Nagura et al. [8]. Pintgen [1, 2] performed simultaneous imaging of the shock front and reaction zone, using schlieren and 2D Laser Induced Fluorescence (LIF), as well as multi-exposure and stereoscopic chemiluminescence imaging.

Jones et al. [9, 10, 11, 12] and Oran et al. [13, 14] used numerical simulations to study the diffraction of detonation and re-ignition process at an abrupt tube diameter increase (180° angle). Layered and uniform H_2-O_2(-Ar) mixtures were modeled. The chemical schemes were either 1-step or 2-step models. Arienti et al. [15] and Nagura et al. [8] performed simulations of detonation diffraction from a channel to an unconfined volume (90° angle). Arienti used a 1-step reaction model characterized by different activation energies whereas Nagura employed a 2-step scheme to model a stoichiometric H_2-air mixture. Khasainov et al. [6] studied the diffraction

of detonation from a channel to a cone. A stoichiometric C_2H_2-O_2 mixture was considered using a 1-step pressure dependent reaction model. Deiterding [16, 17] studied the failure and re-ignition of diffracting detonation in a stoichiometric H_2-O_2 mixture diluted with 70% of Ar. High-resolution numerical simulation with mesh refinement was used. The fluid mechanics were modeled with Euler equations and the reactivity of the mixture was described using a detailed reaction model composed of 34 irreversible reactions and 9 species. Deiterding results are in qualitative agreement with the experimental results of Schultz [4]. Note that these two studies focus mostly on the performance of the mesh refinement technique

From this literature review, we see that most numerical studies have been performed using global (1- or 2-step) kinetic schemes with the exception of Deiterding's work [16, 17]. Even though simple global chemical models enable reproducing the main features of propagating and diffracting detonations, the kinetics parameters are often adjusted to match some particular aspects of the experimental observations. Such an approach cannot provide reliable quantitative comparisons and is limited to a very narrow range of conditions. In addition, very few, if any, side-by-side comparisons were provided for similar mixture compositions, conditions, and measured quantities, and no quantitative assessments were made except for the critical channel height for detonation transmission. The present study aims at performing numerical simulations of detonation diffraction using a high order numerical code with adaptive mesh refinement along with realistic chemical, thermodynamic and spectroscopic models to enable a more realistic comparison with the experimental data of Pintgen in terms of diffracting detonation behaviour and structure for the same mixture compositions, channel height, measured quantities, and, when possible, same pressure. The experiments from Pintgen [1, 2] were selected because they are the only ones that provide imaging for both the shock wave and the reaction zone. In addition, we aim at performing quantitative assessments for a number of relevant diffraction parameters: critical channel height, re-initiation and wall reflection distances, and dynamics of the detonation decoupling process.

2. Numerical model

2.1. Governing equations

We consider the two-dimensional reactive Euler equations

$$\frac{\partial \mathbf{U}}{\partial t} + \frac{\partial \mathbf{F}}{\partial x} + \frac{\partial \mathbf{G}}{\partial y} = \mathbf{S} \tag{1}$$

where $\mathbf{U} = (\rho, \rho u, \rho v, \rho E, \rho Y_i)^{Tr}$ is the vector of conservative variables with ρ the density, u and v the velocity in x and y directions, E the total energy and Y_i the mass fraction of the i^{th} species. Convective fluxes in the x and y direction are $\mathbf{F} = (\rho u, \rho u^2 + p, \rho uv, \rho uE + pu, \rho uY_i)^{Tr}$ and $\mathbf{G} = (\rho v, \rho uv, \rho v^2 + p, \rho vE + pv, \rho vY_i)^{Tr}$, where p is the pressure and Tr superscript is the transpose. The source term vector is $\mathbf{S} = (0, 0, 0, 0, \rho\dot{\omega}_i)^{Tr}$. The source term for the energy equation is zero since the reference energy is included in the total energy E. The

reaction rate $\dot{\omega}_i$ follows Arrhenius laws. Species thermodynamic properties are evaluated using temperature-dependent polynomial expressions [18]. A perfect gas law is assumed with $p{=}\rho RT/\bar{W}$, where R is the perfect gas constant, T the temperature, and $\bar{W}$ the molar mass.

2.2. Numerical method

Euler equations are solved using a finite volume technique on block-structured grids. The numerical fluxes at cell edges are computed using a HLLC Riemann solver [19]. To reach a high level of accuracy and computational efficiency, values of flow variables at cell interfaces are reconstructed using a WENO-5 scheme [20, 21]. It is fifth-order accurate in smooth regions while having sharp (2$\sim$3 grid points), non-oscillatory transitions at discontinuities. The scheme has been implemented and validated against the classical Sod shock test case [22]. Time integration is explicit and uses a third-order Runge-Kutta method [23]. To ensure positivity of mass fractions we have implemented a fifth-order accurate limitation as proposed by Zhang and Shu [24]. The method is based on Hermite-type polynomials and satisfies strict maximum principles without destroying accuracy. A Strang operator splitting is used for accurate coupling between chemistry and convection, which reads $\mathbf{U}^{n+1}{=}\mathcal{L}^C_{\Delta t/2}\mathcal{L}^\chi_{\Delta t}\mathcal{L}^C_{\Delta t/2}\mathbf{U}^n$ where $\mathcal{L}^C$ is the convection operator and $\mathcal{L}^\chi$ the chemical operator. The differential equation $d\mathbf{U}/dt = \mathbf{S}$ is stiff due to the large range of time scale in the detailed chemical reaction mechanism and is consequently solved using an implicit Runge-Kutta-Rosenbrock method with adaptive time-stepping.

2.3. Adaptive Mesh Refinement

An adaptive mesh refinement (AMR) strategy is chosen to adequately resolve the fluid motion and detonation structure. Our code relies on the PARAMESH library [25] which is a community toolkit designed for parallel adaptive mesh. It builds a hierarchy of sub-grids to cover the domain with variable resolution. All the grid blocks have an identical structure, presently a cartesian $8{\times}8$ grid by block, and can be refined until a refinement criterion is fulfilled or a predefined maximum grid level is reached. Each grid block is surrounded by a layer of 3 ghost cells around to impose boundary conditions. During a refinement step, the solution on a refined block is interpolated from the coarser solution using a dimension-by-dimension WENO-5 interpolation. All the blocks are advanced in time with a uniform global time-step given by a Courant number CFL=0.3. The refinement criterion, needed to determine where adaptive refinement/de-refinement is needed, is the Sun-Takayama criterion [26] applied to pressure as well as OH mass fraction. Note that the PARAMESH package manages the creation of grid blocks, builds the associated quad-tree structure and distributes the blocks among processors using MPI.

2.4. Simulation parameters

Detonation propagations are first simulated in a 2D channel with radius R=19 mm to comply with experimental conditions [1]. Boundary conditions are a slip boundary for the wall, a symmetry condition for

centerline and extrapolation conditions at both channel ends. The computation is first initialized by prescribing a high-velocity, high-pressure region until the solution relaxes to a time-average steady state. Then, a small flow disturbance (modified species concentration of the fresh mixture) is imposed so as to trigger the transverse waves intrinsic to propagating detonations. For diffraction studies, the channel solution is eventually mapped onto the diffraction geometry, which consists of the same channel (length about $2.5R$) exiting in a large domain, about $5R$ in each direction. Simulations were performed with the finest resolution equal to 4 μm. Using AMR, the maximum number of cells required for the diffraction geometry is around 4 million as compared to 600 million grid points for a uniform grid at this resolution.

3. Chemical and spectroscopic models

3.1. Chemical reaction model

The reaction model used to perform the simulation is a reduced version of the model of Mével et al. [27, 28], which has been extensively validated against shock-tube, flow and jet-stirred reactor, and burning speed experimental data as well as other combustion related parameters [29, 30, 31, 32, 33]. It is composed of 17 reversible reactions and 9 species, including Ar.

3.2. Laser induced fluorescence model

We have previously applied a laser fluorescence model to ideal 1D (ZND) and 2D unsteady numerical simulations of propagating detonations [2, 34, 35]. A comprehensive description of the model can be found in [2, 34]. Briefly, the 3-level model of Bessler [36] has been chosen as an approximation of LIF process. It considers laser excitation from the ground state (1) to the upper state (2) and fluorescence emission due to transitions from (2) to all possible vibrational and rotational electronic ground states. Based on the experimental configuration used by Pintgen [1, 2], the contributions of the $A^2\ \Sigma^+ \leftarrow X^2\ \Pi$ (1,0) $Q_2(8)$ and $A^2\ \Sigma^+ \leftarrow X^2\ \Pi$ (1,0) $Q_1(9)$ absorption lines, at 35210.25 cm^{-1} (284.0082 nm) and 35210.68 cm^{-1} (284.0047 nm), respectively, were taken into account.

3.3. Chemiluminescence model

To enable a realistic comparison with the multi-exposure chemiluminescence imaging results of Pintgen [2], we have used a chemiluminescence model based on the results of Mével et al. [32]. We assumed that chemiluminescence originates only from the $\left(A^2\sum^+ - X^2\Pi\right)$ transition of the excited hydroxyl radicals. The kinetics of OH* is described by R1: H+O+M=OH*+M; R2: OH*+H_2O=OH+H_2O; and R3: OH*=OH+hν. Applying the quasi-steady-state-approximation to OH*, justified by Mével et al. [32], leads to

$$[OH^*]_{steady-state} = \frac{k_1\,[H]\,[O]\,[M]}{k_2\,[H_2O] + k_{-1}\,[M] + k_3} \tag{2}$$

Using Equation 2, the field of OH* mole fraction can be calculated a posteriori from the fields of temperature, pressure and H, O and H_2O mole fractions. Water vapor is by far the most efficient quencher so it is reasonable to neglect the effect of the other species present in the reaction zone when computing quenching effects using only R2.

4. Results and discussion

4.1. Propagating detonation waves

To simulate the experimental results of Pintgen et al. [2], two conditions have been numerically investigated, (i) a sub-critical case obtained for a stoichiometric H_2-O_2 mixture diluted with 70% Ar at P_1=20-100 kPa (mixture 1); and (ii) a super-critical case obtained for a stoichiometric H_2-O_2 mixture diluted with 50% Ar at P_1=57.5 kPa (mixture 2). In all cases, the initial temperature is 295 K.

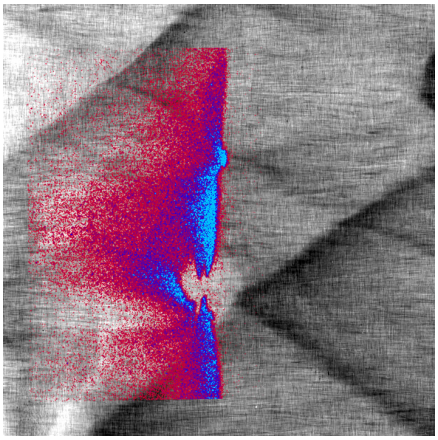

a) Experimental soot foil with superimposed PLIF

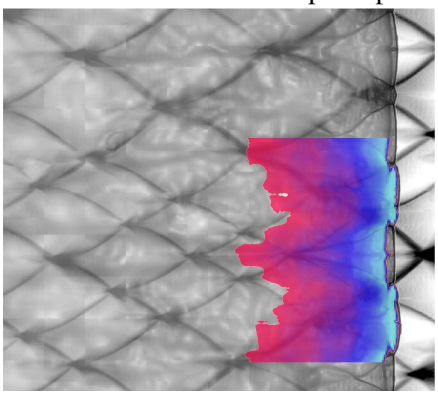

b) Numerical soot foil with superimposed PLIF-schlieren

Figure 1: Experimental [2] and numerical soot foil and superimposed PLIF(-schlieren) images for a propagating detonation. a): $2H_2$-O_2-17Ar, P_1=20 kPa, T_1=294 K, image height=85 mm. b): mixture 2, T_1=295 K, P_1=57.5 kPa, image height=5 mm.

As demonstrated by Jones et al [11], high spatial resolution is required to simulate a diffracting detonation because the cellular structure plays a fundamental role in the qualitative nature, re-ignition or failure, of the diffraction process outcome. Presently, the resolution was increased until the soot foil pattern becomes stable in terms of cell size and regularity. Consequently, all the simulations were performed with a minimum grid size of 4 μm which corresponds to 15 to 90 grid points/induction length (at D_{CJ}), well within the commonly

accepted recommendations [37, 38]. Figure 1 shows an example of experimental superimposed soot foil-PLIF iamge and of numerical soot foil along with instantaneous superimposed schlieren-PLIF images for a detonation propagating in mixture 2 prior to undergoing diffraction. Note that Figure 1 compares different conditions because no experimental cell pattern data are available at conditions similar to those employed in Pintgen et al. diffraction studies [1, 2]. The soot foil exhibits a relatively regular pattern as observed experimentally for this kind of weakly unstable mixture [39]. The schlieren and reaction zone appear as smooth surfaces without the small scale features typical for mixtures with high activation energy [39, 40]. In both the experimental and numerical PLIF fields, well defined keystone features are observed. For mixture 1, the cell width ranges between 1.04 mm at P_1=100 kPa and 3.82 mm at P_1=20 kPa. For mixture 2, the cell width is 0.95 mm. The numerical cell widths are one and a half to four times smaller than the experimental values of Strehlow et al. [41] and Anderson and Dabora (extrapolated) [42]. These differences can be partly explained by the velocity deficit that is always observed in the experiments [39] but is not accounted for in the simulations. We have previously reported for a H_2-N_2O-Ar mixture an increase of a factor of two in the numerical cell width when the detonation velocity in the simulation was decreased by 50 m/s, corresponding to about 2.5% velocity deficit, to match the experimental detonation speed [35]. According to previous studies [39, 43], the maximum possible velocity deficit increases with the regularity of the mixture, up to about 10% for very regular mixtures. Consequently, it could be expected that much better agreement would be obtained for the presently studied mixtures in terms of cell width by accounting for realistic velocity deficits. This aspect is however beyond the scope of our study and the numerical cell width obtained at D_{CJ} have been used as a reference length scale.

4.2. Diffracting detonation waves

Figure 2 and Figure 3 present a comparison between the experimental [2] and simulated superimposed schlieren-PLIF and schlieren-OH images obtained for mixtures 1 and 2, respectively.

The two different diffraction regimes observed experimentally, sub-critical for mixture 1 and super-critical for mixture 2, are reproduced in the simulations with the qualitative agreement between the experimental and synthetic images based on the numerical results. In both mixture 1 and 2, the LIF field appears as a relatively thin layer with a maximum intensity at the reaction zone front. The intensity of the signal decreases very sharply due to the strong absorption of the laser light and the regions of high OH concentration away from the detonation front do not appear as region of high LIF intensity, consistent with our previous results for propagating detonations [34]. For mixture 1, the uncoupled reaction zone exhibits a pronounced sawtooth shape as observed experimentally. The boundary of the sawtooth structures marks the contact surface between the quenched reaction zone with high OH concentration and the shocked but unreacted region with low OH concentration. For mixture 2, the maximum LIF signal is observed at the undisturbed detonation front and at the front of the fan-like

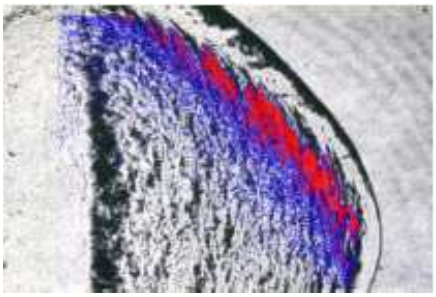

a) Experimental schlieren-PLIF

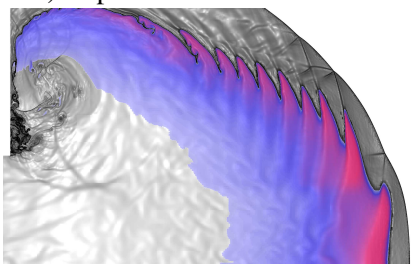

b) Numerical schlieren-PLIF

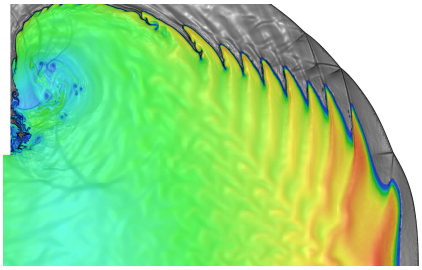

c) Numerical schlieren-OH

Figure 2: Experimental [2] and numerical schlieren-PLIF and schlieren-OH images of a sub-critical detonation diffraction in mixture 1. Experiments: T_1=295 K; P_1=100 kPa; image height=53 mm. Simulations: T_1=295 K; P_1=20 kPa; image height=40 mm.

structure [8] which is created by transverse waves propagating outward along the front. In the simulation, the front of the transverse detonation (at the upper boundary of the "fan") appears as a zone of low LIF intensity whereas the OH field exhibits high concentration at this location. This is due to the strong absorption of the laser light by the OH just behind the fan structures. Note that in the experiment (Figure 3 a), the OH field behind the transverse detonation is visible due to the limited extent of the light sheet in the experimental setup. Future

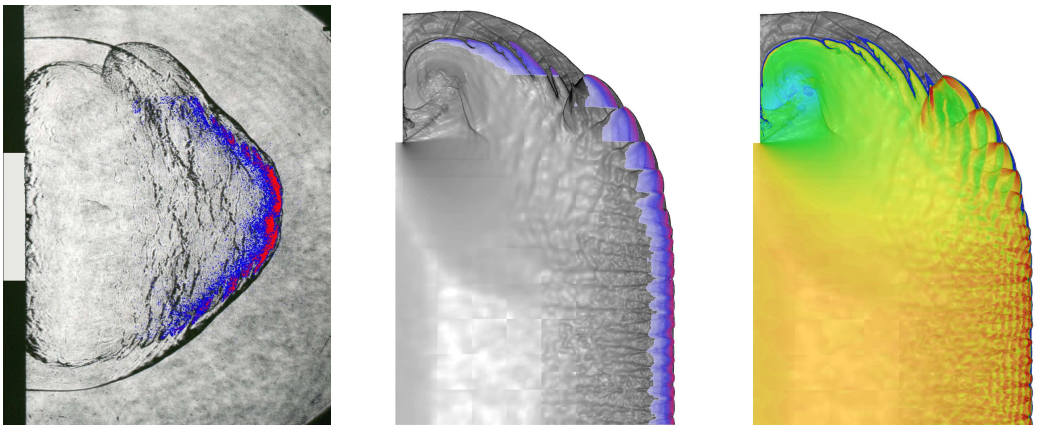

a) Experimental schlieren-PLIF b) Numerical schlieren-PLIF c) Numerical schlieren-OH

Figure 3: Experimental [2] and numerical schlieren-PLIF or schlieren-OH images of a super-critical detonation diffraction in mixture 2. a): T_1=295 K; P_1=57.5 kPa; image height=125 mm. b) and c): T_1=295 K; P_1=57.5 kPa; image height=29 mm.

experimental studies should consider other light sheet configurations to visualize this feature. The uncoupled reaction zone located behind the diffracting shock wave does appear as a zone of low LIF intensity with a less pronounced sawtooth shape consistent with the OH field.

In both the failure and re-ignition cases, the evolution of the diffracting detonation wave observed in the simulation is consistent with previous experimental and numerical results. As the detonation exits into the unconfined volume, diffraction of the wave in the vicinity of the corners results in the reaction zone decoupling almost instantaneously from the leading shock. The central portion of the detonation front remains quasi-planar but the portion of the front that is undisturbed decreases as the expansion waves travel toward the axis of symmetry.

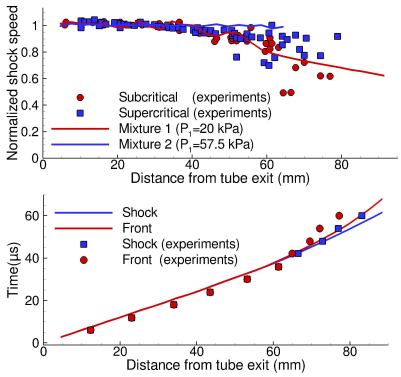

Figure 4: Experimental [2] and numerical normalized (D/D_{CJ}) shock speed (top) and shock and reaction fronts trajectories for the sub-critical case (bottom). Conditions: T_1=295 K; P_1=20-100 kPa.

For mixture 1, the residual transverse waves or spontaneous processes at hot spots [12] fail to re-ignite the unreacted gas volume which was shocked by the diffracting shock. The geometry of the detonation progressively evolves from planar to spherical and eventually, the reaction zone completely decouples from the leading shock. Figure 4 shows the evolution of (top) the detonation front velocity as well as (bottom) the trajectory of the flame and shock fronts. The simulation reproduces the evolution of the normalized shock velocity at the channel axis as decoupling is taking place. At a distance of 70 mm, a velocity of 0.7 D_{CJ} is predicted, in good agreement with the experimental measurements [2]. It is also shown in Figure 4 (bottom), that the trajectory of the simulated flame and shock fronts agree within a few mm with the experimental values even though the decoupling appears slightly faster in the experiment than in the simulation.

For mixture 2, the central part of the detonation front remains undisturbed and quasi-planar throughout the simulation. Figure 4 (top) indicates that the normalized shock velocity at the channel axis remains essentially constant at D_{CJ} during the propagation of the diffracting detonation in the unconfined volume. In the unreacted but shocked volume, a reactive fan-like structure readily establishes due to the compression by the transverse waves. Eventually, a transverse detonation is formed between the leading shock and burnt gas and propagates

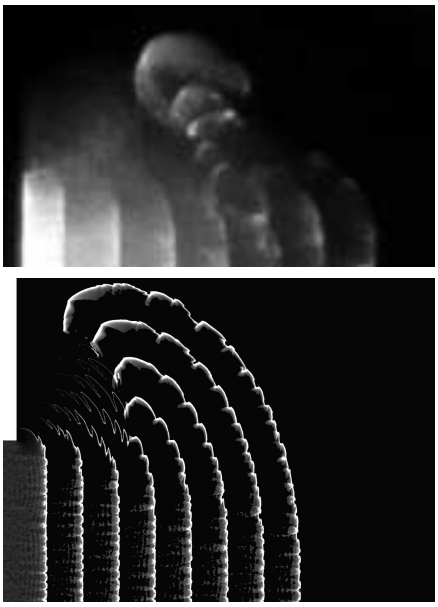

Figure 5: Experimental [2] (top) and numerical (bottom) multi-exposure chimiluminescence images of a super-critical detonation diffraction in mixture 2. Top: T_1=295 K; P_1=57.5 kPa; image height=55 mm; $\Delta(t_{expo})$=6 μs. Bottom: T_1=295 K; P_1=57.5 kPa; image height=40 mm; $\Delta(t_{expo})$=2 μs.

toward the wall. Figure 5 shows a comparison between the multi-exposure chemiluminescence (OH*) images obtained experimentally [2] and the synthetic image obtained by processing the simulations. The trajectory of the boundary of the expansion wave as well as the strong transverse detonation are clearly visible in both images. In these images, the transverse detonation front appears as a region of intense chemiluminescence indicating rapid chemical activity resulting in radical formation. The horizontal distance from the propagation channel exit at which re-initiation of the diffracting detonation is observed is shown in Figure 6 (top) for a range of P_1 for both mixtures. Note that the numerical cell size has been used for the normalization of the numerical distance to re-initiation. This distance is relatively constant at about 12-15 λ which is in reasonable agreement with the value of 11 λ reported by Nagura et al. [8]. The transverse detonation eventually reflects at the wall at some distance from the corner. Numerical results for the wall reflection distances are shown in Figure 6 (bottom) for a range of initial pressure along with the limiting values obtained by Nagura et al. [8] for a wide variety of mixtures including both weakly and highly unstable cases. In our simulations, the wall reflection distances are between 12 and 14 λ which is consistent with Nagura et al. experimental data range, 10 to 15 λ. The present simulations reproduce slightly better the reflection distance as compared to Nagura et al. calculations with an estimated normalized distance on the order of 20 λ.

In order to obtain a sub-critical numerical simulation outcome for mixture 1, the initial pressure had to be set to a much lower value than in the experiments, 20 kPa against 100 kPa. The channel height to cell width ratio for critical conditions is found to be between 10.0 and 11.3 for mixture 1. Jones et al. [11] report a critical channel height in the range H_c=3-7 λ, consistent with experimental data for high aspect ratio rectan-

gular channels [44]. Deiterding [17] observed a critical channel height of approximately H_c=10λ, which is in agreement with the value reported for square channels [44]. The present and previous results indicate that the difference between the critical ratios for detonation transmission between the simulations and experiments are due to the difference of geometry, with a high aspect ratio channel for the simulations versus a circular tube for the experiments. The geometry of the channel influences the three-dimensional structure of the expansion wave that results in the quenching of the diffracting detonation. In order to reproduce the correct shape of the expansion wave, three-dimensional simulations would be needed but unfortunately, these are still not accessible due to limitations in computational resources particularly when a realistic chemical reaction model is used. The lack of experimental visualization of detonation diffracting from squared and rectangular channels [44] prevents any closer comparison than the ones presented in the paper. Although the critical channel height is known to increase as the instability level of a detonation decreases [45], this effect is not well captured by the simulation and calculations with mixtures with higher effective activation energy, such as H_2-N_2O, should be performed to examine this aspect.

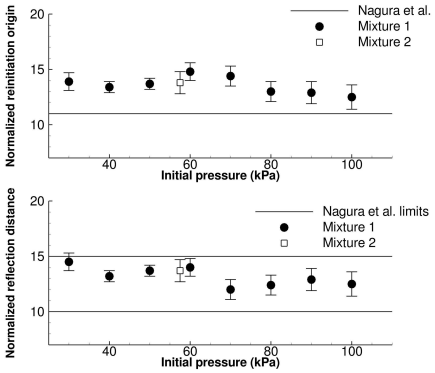

Figure 6: Experimental [8] and numerical a) re-initiation and b) wall reflection distances. T_1=295 K; P_1=30-100 kPa. Distances are normalized by cell width.

5. Conclusions

In the present study, the diffraction of detonation waves in hydrogen-oxygen mixtures has been investigated using 2D numerical simulations performed with an high-order AMR Euler solver and a realistic thermochemical scheme. The numerical results demonstrate a reasonable agreement with previously obtained experimental and numerical data in terms of diffracting detonation behaviour and structure. Key features observed in the experimental PLIF and chemiluminescence images were reproduced by employing molecular models and spectroscopic considerations. It is shown that performing a meaningful comparison with these visualizations demands the use of up-to-date spectroscopic models that we previously developed because the OH PLIF and OH* chemiluminescence signals are not directly related, or not related at all, to the OH concentration [35, 34, 32]. The reasonable agreement between synthetic and experimental PLIF and OH* images indicate that many of the features of diffraction are controlled by inviscid gas dynamics interactions and chemical reaction processes.

We recognize that in some cases, diffusion across contact surface of shear layers may play a significant role, particularly in the near critical regime. Obviously, these aspects are outside the capability of the present inviscid simulations. A number of macroscopic features of detonation diffraction, including re-initiation and wall reflection distances, were quantitatively reproduced by the simulations. Future work will focus on the simulation of detonation diffraction in mixtures with high effective activation energy such as hydrogen-nitrous oxide mixtures.

Acknowledgments

The authors would like to thank Alban Combe (Herakles) for his help on AMR.

List of Figures

References

[1] F. Pintgen, J. E. Shepherd, Combust. Flam 156 (2009) 655–677.

[2] F. Pintgen, Detonation diffraction in mixtures with various degrees of instability, Ph.D. thesis, California Institute of Technology, 2004.

[3] M. Arienti, A numerical and analytical study of detonation diffraction, Ph.D. thesis, California Institute of Technology, 2003.

[4] E. Schultz, Detonation diffraction through an abrupt area expansion, Ph.D. thesis, California Institute of Technology, 2000.

[5] Y. Zeldovich, S. Kogarko, N. Simonov, Sov. Phys. Tech. Phys. 1 (1956) 1689–1713.

[6] B. Khasainov, H.-N. Presles, D. Desbordes, P. Demontis, P. Vidal, Shock Waves 14 (2005) 187–192.

[7] J. Meredith, H. Ng, J. Lee, Shock Waves 20 (2010) 449–455.

[8] Y. Nagura, J. Kasahara, Y. Sugiyama, A. Matsuo, Proc. Combust. Inst. 34 (2013) 1949–1956.

[9] D. A. Jones, M. Sichel, E. Oran, G. R., Proc. Combust. Inst. 23 (1990) 1805–1811.

[10] D. A. Jones, M. Sichel, E. Oran, Shock Waves 5 (1995) 47–57.

[11] D. A. Jones, G. Kemister, E. Oran, S. M., Shock Waves 6 (1996) 119–129.

[12] D. A. Jones, G. Kemister, N. Tonello, E. Oran, M. Sichel, Shock Waves 10 (2000) 33–41.

[13] E. Oran, D. Jones, M. Sichel, Proc. R. Soc. A 436 (1992) 267–297.

[14] E. Oran, J. Boris, D. Jones, M. Sichel, Prog. Astronaut. Aeronaut. 153 (1993) 241–252.

[15] M. Arienti, J. Shepherd, J. Fluid Mech. 529 (2005) 117–146.

[16] R. Deiterding, Parallel adaptive simulation of multi-dimensional detonation structures, Ph.D. thesis, Technischen Universitat Cottbus, 2003.

[17] R. Deiterding, J. Combust. 2011 (2011) ID 738969.

[18] R. Kee, G. Rupley, J. Miller, Chemkin II : A Fortran chemical kinetics package for the analysis of gas phase chemical kinetics, Technical Report, Tech. Rep. SAND89-8009B, Sandia National Laboratories, 1992.

[19] E. F. Toro, Riemann solvers and numerical methods for fluid dynamics: a practical introduction, Springer Science & Business Media, 2009.

[20] C.-W. Shu, Essentially non-oscillatory and weighted essentially non-oscillatory schemes for hyperbolic conservation laws, Springer, 1998.

[21] G.-S. Jiang, C.-W. Shu, J. Comput. Phys. 126 (1996) 202–228.

[22] G. A. Sod, J. Comput. Phys. 27 (1978) 1–31.

[23] C. Shu, S. Osher, J. Comput. Phys. 77 (1988) 439–471.

[24] X. Zhang, C.-W. Shu, J. Comput. Phys. 229 (2010) 3091–3120.

[25] P. MacNeice, K. M. Olson, C. Mobarry, R. de Fainchtein, C. Packer, Comput. Phys. Commun. 126 (2000) 330–354.

[26] M. Sun, K. Takayama, J. Comput. Phys. 150 (1999) 143–180.

[27] R. Mével, S. Javoy, F. Lafosse, N. Chaumeix, G. Dupré, C. E. Paillard, Proc. Combust. Inst. 32 (2009) 359–366.

[28] R. Mével, S. Javoy, G. Dupré, Proc. Combust. Inst. 33 (2011) 485–492.

[29] R. Mével, Etude de mécanismes cinétiques et des propriétés explosives des mélanges hydrogène-protoxyde d'azote et silane-protoxyde d'azote. Application à la sécurité industrielle, Ph.D. thesis, Université d'Orléans, 2009.

[30] R. Mével, F. Lafosse, N. Chaumeix, G. Dupré, C.-E. Paillard, Int. J. Hydrogen Energ. 34 (2009) 9007–9018.

[31] B. Zhang, H. D. Ng, R. Mével, J. H. S. Lee, Int. J. Hydrogen Energ. 36 (2011) 5707–5716.

[32] R. Mevel, S. Pichon, L. Catoire, N. Chaumeix, C. E. Paillard, J. E. Shepherd, Proc. Combust. Inst. 34 (2013) 677–684.

[33] S. Coronel, R. Mevel, S. P. M. Bane, J. E. Shepherd, Proc. Combust. Inst. 34 (2013) 895–902.

[34] R. Mével, D. Davidenko, J. Austin, F. Pintgen, J. E. Shepherd, Int. J. Hydrogen Energ. 39 (2014) 6044–6060.

[35] R. Mével, D. Davidenko, F. Lafosse, N. Chaumeix, G. Dupré, C. E. Paillard, J. E. Shepherd, Combust. Flame 162 (2015) 1638–1649.

[36] G. Bessler, C. Schulz, V. Sick, J. W. Daily, Proc. US Combust. Meet. 3 (2003) 6.

[37] E. S. Oran, J. W. Weber, E. I. Stefaniw, M. H. Lefebvre, J. D. Anderson, Combust. Flame 113 (1998) 147–163.

[38] G. J. Sharpe, J. Fluid Mech. 447 (2001) 31–51.

[39] J. M. Austin, The role of instability in gaseous detonation, Ph.D. thesis, California Institute of Technology, 2003.

[40] J. M. Austin, F. Pintgen, J. E. Shepherd, Proc. Combust. Inst. 30 (2005) 1849–1857.

[41] R. Strehlow, R. Liangminas, R. Watson, J. Eyman, Proc. Combust. Inst. 11 (1967) 683–692.

[42] T. J. Anderson, E. K. Dabora, Proc. Combust. Inst. 24 (1992) 1853–1860.

[43] I. Moen, J. Funk, S. Ward, G. M. Rude, P. Thibault, Prog. Astronaut. Aeronaut. 94 (1984) 55?79.

[44] W. Benedick, R. Knystautas, J. Lee, Prog. Astronaut. Aeronaut. 94 (1984) 546–555.

[45] J. E. Shepherd, I. O. Moen, S. B. Murray, P. A. Thibault, Proc. Combust. Inst. 21 (1986) 1649–1658.